Journal of Non-Newtonian Fluid Mechanics 285 (2020) 104393

Contents lists available at ScienceDirect

Journal of Non-Newtonian Fluid Mechanics

journal homepage: www.elsevier.com/locate/jnnfm

Flow of a Bingham fluid in a pipe of variable radius

Lorenzo Fusi [a], Kostas D. Housiadas [b], Georgios C. Georgiou [c,*]

[a] Università degli Studi di Firenze, Dipartimento di Matematica e Informatica "Ulisse Dini", Viale Morgagni 67/a, 50134 Firenze, Italy
[b] Department of Mathematics, University of the Aegean, Karlovasi 83200, Samos, Greece
[c] Department of Mathematics and Statistics, University of Cyprus, P.O. Box 20537, 1678 Nicosia, Cyprus

ARTICLE INFO

Keywords:
Bingham plastic
Axisymmetric poiseuille flow
Lubrication solution
Converging/diverging tubes
Undulating tubes
Stenosis

ABSTRACT

We extend a method developed by Fusi and Farina (Appl. Math. Comp. 320, 1–15, 2018) to obtain semi-analytical lubrication-approximation solutions for the flow of a Bingham-plastic in a tube of variable radius. The proposed method is applicable provided that the unyielded core extends continuously from the inlet to the outlet. It turns out that the variable radius of the latter core obeys a stiff integral-algebraic equation which is solved both numerically and asymptotically. The pressure distribution is then obtained integrating a 1st-order ODE and the velocity components are computed using analytical expressions. Converging or diverging either linearly or exponentially, undulating and stenosed tubes are considered. The effects of the shape of the wall on the yield surface which separates the yielded region from the unyielded core and on the pressure difference required to drive the flow are investigated and discussed. The results show that the effect of the wall variation amplitude is greatly amplified as the volumetric flow rate (or, equivalently, the imposed pressure difference driving the flow) increases. It is also demonstrated that the pressure difference needed to achieve a given volumetric flow rate in a converging pipe is always higher than that for a diverging one.

1. Introduction

Yield-stress or viscoplastic materials include various classes of materials, such as colloidal gels, emulsions, soft glassy materials, and jammed noncolloidal suspensions, foams, and paints [1,2]. They have received considerable attention in the past few decades as they appear in many processes of industrial importance, such as food processing, pharmaceutics, cosmetics, and oil-drilling and transport [3], in construction, in geophysical flows and in biological flows [4]. Ideal yield-stress fluids behave as solids below the yield stress, τ_0^*, and as fluids otherwise. The most popular constitutive equation describing viscoplastic behavior is the Bingham model [5]. In axial flow in a tube, this model is simplified as follows:

$$\begin{cases} \dfrac{\partial v_z^*}{\partial r^*} = 0, & \tau^* \le \tau_0^* \\ \tau_{rz}^* = \operatorname{sign}\left(\dfrac{\partial v_z^*}{\partial r^*}\right)\tau_0^* + \mu^* \dfrac{\partial v_z^*}{\partial r^*}, & \tau^* > \tau_0^* \end{cases} \tag{1}$$

where v_z^* is the axial velocity component, τ_{rz}^* is the shear stress, $\tau^* = |\tau_{rz}^*|$, and μ^* is the plastic viscosity. Note that in this paper symbols with stars denote dimensional quantities.

The Bingham model along with its Herschel-Bulkley variant (i.e. its power-law generalization) are ideal yield-stress models, i.e. the shear stress depends only on the imposed shear rate. Consequently, these models cannot describe thixotropic or elastic behavior [2]. Solving ideal viscoplastic flows requires the determination of the unyielded ($\tau^* \le \tau_0^*$) and yielded ($\tau^* > \tau_0^*$) zones where the two branches of the two-branch constitutive equation apply. This task is easy in simple unidirectional flows, such as in Poiseuille and Couette flows, where the unyielded region is a cylindrical core moving axially at a constant speed in the former and rotating at a constant angular velocity in the latter case; the radius of the unyielded core is computed by solving a nonlinear algebraic equation. However, the determination of yielded regions becomes extremely difficult especially in two- and three-dimensional flows [2], e.g. in flows in channels or tubes of varying width or radius, respectively, or in standard Poiseuille flows when the rheological parameters are pressure dependent [6,7].

Fusi et al. [8] proposed a lubrication approximation method for solving Bingham-plastic flows in symmetric long channels of non-constant width. With their method the integral form of the momentum balance over the unyielded core (the unknown width of which

* Corresponding author.
E-mail address: georgios@ucy.ac.cy (G.C. Georgiou).

https://doi.org/10.1016/j.jnnfm.2020.104393
Received 11 March 2020; Received in revised form 4 June 2020; Accepted 4 September 2020
Available online 19 September 2020

also varies with the axial coordinate) is employed and the zero-order perturbation equations in terms of the aspect ratio of the channel, which serves as the small parameter of the perturbation, are solved. The pressure is calculated by solving a first-order ordinary differential equation (ODE) and then the yield surface and the two velocity components are calculated using explicit analytical expressions in terms of the pressure and the wall shape function. The fact that the yield surface is calculated explicitly is one advantage of the method. Moreover, the method yields the correct shape of the yield surface at zero-order, which means that the yield surface contracts if the wall expands and vice versa. This might be counter-intuitive but necessary for mass-conservation; given that the plug moves at a constant speed along the channel, it contracts when the channel expands and vice versa [9].

The standard lubrication approximation methods cannot yield this result at zero-order; they predict instead that the plug speed varies slowly in the main flow direction, a phenomenon known as the lubrication approximation paradox [9,10]. On the other hand, the method of Fusi et al. [8] is applicable only when the unyielded region extends continuously from the inlet to the outlet of the tube, i.e. above a critical pressure difference at which flow occurs and below the critical pressure difference at which the unyielded core breaks. More specifically, if the pressure difference between the inlet and the outlet planes of a converging channel is increased, then the yield surface moves towards the symmetry axis and eventually the expanding plug breaks at the inlet plane. If the pressure difference is decreased, then the volumetric flow rate is reduced and the yield surface moves towards and eventually reaches the wall; at this critical value the speed of the unyielded core vanishes due to the no-slip boundary condition and therefore there is no flow. Hence, the method is applicable only between these two critical values of the imposed pressure difference. Similar arguments also hold for an expanding channel; at a critical value of the pressure difference the contracting core breaks at the exit plane. It is also easy to deduce that the lubrication approximation method is only applicable for small or moderate changes of the channel width. For example, increasing the width difference between the inlet and outlet of a converging channel results in faster expansion of the unyielded core which eventually touches the wall so that there is no flow.

Panaseti et al. [6] extended the method of Fusi et al. [8] to solve the flow of Herschel-Bulkley fluids with pressure-dependent consistency index and yield stress and derived analytical solutions for channels with linearly varying width. Subsequently, Panaseti et al. [11] considered the more general case of asymmetric horizontal channels, where the unyielded core moves not only horizontally but also vertically, depending on the two functions describing the shapes of the upper and lower walls.

Fusi and Farina [12] extended the lubrication-approximation method for axisymmetric viscoplastic flows in long tubes of varying radius. Their method has been applied by Housiadas et al. [7] to solve the flow in a tube of constant radius of a Bingham plastic with yield stress and plastic viscosity varying linearly with pressure. Applying the perturbation method results in a system of a first-order ODE and an algebraic equation for the pressure distribution and the yield surface, which is not constant due to the pressure dependency of the rheological parameters. The latter system was solved both numerically using a pseudospectral method and by means of simple perturbation method, which allowed the derivation of some asymptotic results.

The objective of the present work is to apply the method of Fusi and Farina [12] in order to study the flow of a Bingham plastic in tubes of varying radius, e.g. expanding or contracting tubes, or tubes with a stenosis. We focus only on the effect of the wall function on the solution and thus the rheological parameters of the Bingham plastic model are assumed to be constant (i.e. pressure independent). It should be pointed out that with the exception of a few studies with axisymmetric contractions and/or expansions relevant to polymer processing [13,14], most studies with uneven walls concern planar geometries ([2] and references therein). To our knowledge, the only lubrication-approximation studies of viscoplastic flow in axisymmetric geometries have been carried out with the method of Fusi and Farina [12], where the flow problem was formulated and solved only in the case of a small variation of the radius, or its extensions by Housiadas et al. [7], where the radius of the tube was taken to be constant. In the present work, the axisymmetric flow is solved numerically at the leading order of the lubrication approximation allowing bigger variations in the radius. It seems that the resulting simplified equations are more difficult to solve in cylindrical coordinates than in Cartesian ones. For example, there is a striking difference between the flows of a Bingham fluid with pressure-dependent rheological parameters in long channels and tubes of constant width and radius, respectively. In the planar case the width of the unyielded core is constant, whereas in the case of tubes the radius of the core may be increasing or decreasing depending on the relative values of the yield-stress and plastic-viscosity growth parameters [6,7]. Despite the scarcity of many published works, studying the flow of yield-stress fluids in tubes of variable radius is of interest in many applications, such as blood flow in stenoses [15], flow through membranes with conical pores [16], and non-Darcy flow through porous media using pore network modelling with cylindrical throats and/or converging/diverging pore space [17].

The paper is organized as follows. The derivation of the model is described in Section II. Unlike the flow in a symmetric channel of variable width [6], the axisymmetric flow results in a stiff algebraic/integral equation for the yield radius. Then, all the field variables can be easily calculated via analytical expressions. We also derive an approximate analytical solution, i.e. a perturbation solution in terms of the maximum variation of the tube radius, and use it to validate the numerical method. The results are presented and discussed in Section III, where the effects of the yield stress on the pressure difference required to drive the flow and on shape of the yield surface are investigated. The effect of the shape of the wall is also studied by producing results for linearly or exponentially converging/diverging pipes as well as for undulating and stenosed pipes. Finally, concluding remarks are given in Section IV.

2. Mathematical model and solution

We consider the steady-state, axisymmetric flow of an incompressible Bingham plastic in a tube of variable radius $h^* = h^*(z^*)$ and length L^*, employing cylindrical coordinates as illustrated in Fig. 1. Gravity and other external forces are neglected, and the flow is assumed to be driven solely by the pressure difference $\Delta p^* = p^*_{in} - p^*_{out}$ between the inlet and the outlet planes. It is further assumed that the unyielded core (where $\tau^* \leq \tau^*_0$) extends from the inlet to the outlet plane and thus the function $\sigma^* = \sigma^*(z^*)$ describing the yield surface is continuous for $0 \leq z^* \leq L^*$. With the above assumptions the velocity vector is of the form $\mathbf{v}^* = v^*_r(r^*, z^*)\boldsymbol{e}_r + v^*_z(r^*, z^*)\boldsymbol{e}_z$.

The lubrication approximation method is described in detail in [7]. Basically, the equations of motion in the absence of external forces along with the non-trivial extra stress components apply in the yielded region

$$D^* \equiv \{(r^*, z^*, \theta) |\ r^* \in [\sigma^*, h^*], z^* \in [0, L^*],\ \theta \in [0, 2\pi)\}$$

The unyielded region

$$\Omega^* \equiv \{(r^*, z^*, \theta) | r^* \in [0, \sigma^*], z^* \in [0, L^*],\ \theta \in [0, 2\pi)\}$$

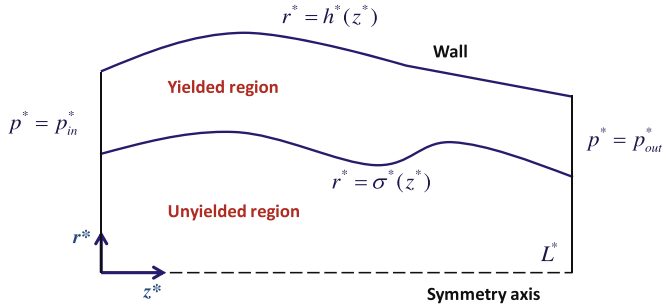

Fig. 1. Geometry and symbol definitions for viscoplastic flow in a tube of variable radius $r^* = h^*(z^*)$.

moves in the z-direction as a solid, i.e. at a constant axial velocity v_c^*.

We indicate here that the method proposed below is applicable when $0 < \sigma^*(z^*) < h^*(z^*)$, i.e. between a lower critical pressure difference at which the yield surface touches the wall ($\sigma^*(z_c^*) = h^*(z_c^*)$ at a point z_c^*) and, consequently, the axial velocity of the unyielded core vanishes due to the no-slip boundary condition and un upper critical pressure difference at which the unyielded core breaks ($\sigma^*(z_c^*) = 0$).

We non-dimensionalize the governing equations by scaling z^* by L^*, r^* and σ^* by $R^* \equiv h^*(0)$, $(p^* - p^*_{out})$and the pressure difference $\Delta p^* = p^*_{in} - p^*_{out}$ by $\tau_0^* L^*/R^*$, v_z^* by $\tau_0^* R^*/\mu_0^*$, v_r^* by $\tau_0^* R^{*2}/(L^*\mu_0^*)$, and the extra-stress components by τ_0^* and dropping the stars for the dimensionless parameters. For long tubes, the aspect ratio $\varepsilon \equiv R^*/L^*$ is a small parameter, $0 < \varepsilon < < 1$ and if $\Delta p = O(1)$ then a lubrication type approximation can be utilized to simplify the governing equations and accompanying auxiliary conditions. It turns out that at zero-order, the pressure p is independent of the radial coordinate, r, and the dimensionless constitutive equation reads:

$$\begin{cases} \dfrac{\partial v_z}{\partial r} = 0, & \tau_{rz} \le 1 \\ \tau_{rz} = -1 + \dfrac{\partial v_z}{\partial r}, & \tau_{rz} > 1 \end{cases} \tag{2}$$

Note that variables or symbols without a star denote dimensionless quantities. In the yielded region D, the shear stress is given by:

$$\tau_{rz} = \frac{p'}{2}\left(r - \frac{\sigma^2}{r}\right) - \frac{\sigma}{r} \tag{3}$$

where hereafter the prime denotes derivative with respect to z. We also drop the explicit dependence of σ, $h$and p on z. The integral balance of linear momentum in Ω leads to the following equation:

$$\int_0^1 \sigma\left(1 + \frac{p'\sigma}{2}\right)dz = 0 \tag{4}$$

Substituting Eq. (2) into Eq. (3), integrating with respect to r and applying the no-slip boundary condition at the wall, $v_z(h(z), z) = 0$, we get the following expression for the axial velocity component:

$$v_z(r,z) = \frac{p'}{4}\left(r^2 - h^2 - 2\sigma^2 \ln\frac{r}{h}\right) - h + r - \sigma \ln\frac{r}{h} \tag{5}$$

The constant velocity of the unyielded core can be found as $v_c = v_z(\sigma(z), z)$:

$$v_c = \frac{p'}{4}\left(\sigma^2 - h^2 - 2\sigma^2 \ln\frac{\sigma}{h}\right) - h + \sigma - \sigma \ln\frac{\sigma}{h} \tag{6}$$

The radial velocity component is calculated by integrating the continuity equation as follows:

$$v_r(r,z) = \frac{1}{r}\int_r^{h(z)} \frac{\partial}{\partial z}(\xi v_z(z,\xi))\, d\xi \tag{7}$$

Given that v_c is constant, $dv_c/dz = 0$, yields an expression for the second derivative of p. This expression is used to eliminate p'' that appears in Eq. (7). Then, integrating and rearranging give:

$$v_r(r,z) = \frac{f_1(z,r) + f_2(z,r)\, h'}{4r\left[h^2 - \sigma^2 + 2\sigma^2 \ln(\sigma/h)\right]} \tag{8}$$

where

$$f_1(r,z) = (1 + p'\sigma)\sigma'\left[\left(h^2 - r^2\right)^2 \ln\frac{\sigma}{h} + \left(h^2 - \sigma^2\right)\left(h^2 - r^2 + 2r^2 \ln\frac{r}{h}\right)\right] \tag{9}$$

and

$$f_2(r,z) = \left(1 - \frac{\sigma}{h}\right)\left[1 + \frac{p'h}{2}\left(1 + \frac{\sigma}{h}\right)\right]\left[r^4 - h^4 - 4\sigma^2\left(h^2 - r^2\right)\ln\frac{\sigma}{h} - 4\sigma^2 r^2 \ln\frac{r}{h}\right] \tag{10}$$

Since the flow is incompressible, the constant volumetric flow rate is found as follows:

$$\begin{aligned} Q &= 2\int_0^{h(z)} v_z(r,z) r dr = 2\int_0^{\sigma(z)} v_c\, r dr + 2\int_{\sigma(z)}^{h(z)} v_z(r,z) r dr \\ &= \sigma^2 v_c + 2\int_{\sigma(z)}^{h(z)} v_z(r,z) r dr \end{aligned} \tag{11}$$

Substituting Eq. (5) into Eq. (11) and carrying out the integration, we get:

$$Q = \frac{(h-\sigma)^2\left[(h+\sigma)^2 v_c + \frac{1}{3}(h+2\sigma)\left(h^2 - \sigma^2\right) + \frac{1}{3}\sigma\left(3h^2 + 2h\sigma + \sigma^2\right)\ln\frac{\sigma}{h}\right]}{2\left(h^2 - \sigma^2 + 2\sigma^2 \ln\frac{\sigma}{h}\right)} \tag{12}$$

The system of the first-order ODE Eq. (6) and the algebraic Eq. (12) is accompanied with the following three auxiliary conditions:

$$p(0) = \Delta p, \quad p(1) = 0, \quad \int_0^1 \sigma\left(1 + \frac{p'\sigma}{2}\right)dz = 0 \tag{13}$$

Next, we introduce new variables $\tilde{r} \equiv r/h$, $\tilde{\sigma} \equiv \sigma/h$; thus $0 < \tilde{\sigma}(z) \le \tilde{r} \le 1$. Then, Eq. (6) becomes:

$$\frac{v_c}{h} = \frac{p'h}{4}\left(\tilde{\sigma}^2 - 1 - 2\tilde{\sigma}^2 \ln\tilde{\sigma}\right) - 1 + \tilde{\sigma} - \tilde{\sigma}\ln\tilde{\sigma} \tag{14}$$

Similarly, the volumetric flow rate is given by:

$$Q = \frac{(1-\tilde{\sigma})^2 h^3\left[(1+\tilde{\sigma})^2 \frac{v_c}{h} + \frac{1}{3}(1+2\tilde{\sigma})(1-\tilde{\sigma}^2) + \frac{\tilde{\sigma}}{3}(3 + 2\tilde{\sigma} + \tilde{\sigma}^2)\ln\tilde{\sigma}\right]}{2(1 - \tilde{\sigma}^2 + 2\tilde{\sigma}^2 \ln\tilde{\sigma})} \tag{15}$$

In terms of the new variables, the auxiliary conditions in Eq. (13) reduce to:

$$\begin{aligned} &p(0) = \Delta p, \\ &p(1) = 0, \\ &\int_0^1 \tilde{\sigma} h\left(1 + \frac{p'\tilde{\sigma}h}{2}\right)dz = 0 \end{aligned} \tag{16}$$

Although Eqs. (14)-(16) constitute a closed system of equations, we can proceed further by solving Eq. (14) for p':

$$p' = -\frac{4(h + v_c - h\tilde{\sigma} + h\tilde{\sigma}\ln\tilde{\sigma})}{h^2(1 - \tilde{\sigma}^2 + 2\tilde{\sigma}^2\ln\tilde{\sigma})} \tag{17}$$

Substituting Eq. (17) in the last condition of Eq. (16), one gets:

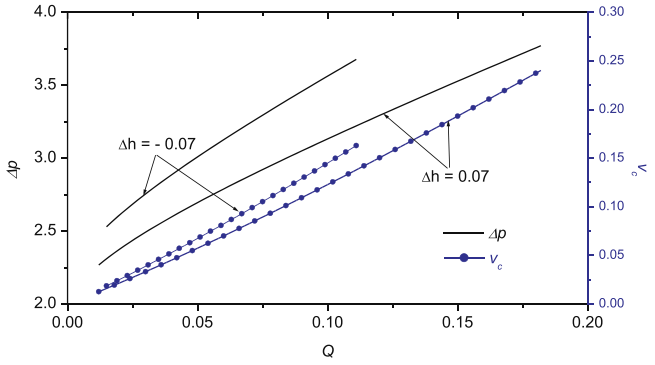

(a)

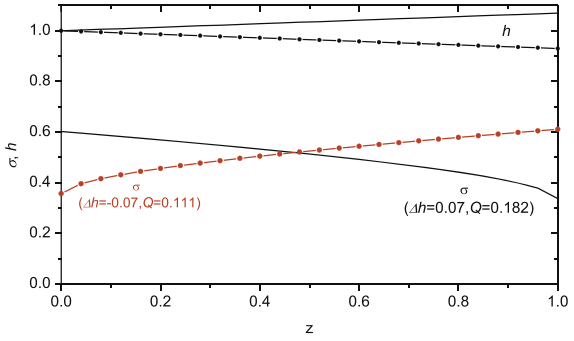

(b)

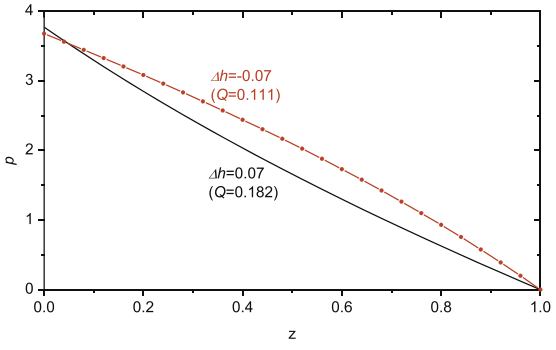

(c)

Fig. 2. Results for linearly converging/diverging pipes with $\Delta h = \pm 0.07$: (a) Δp (continuous lines) and v_c (lines with dots) vs Q; (b) Yield surfaces for $Q = 0.111 (\Delta h = -0.07)$ and $Q = 0.182 (\Delta h = 0.07)$; (c) Pressure distributions for $Q = 0.111 (\Delta h = -0.07)$ and $Q = 0.182 (\Delta h = 0.07)$. The tube radius is given by $h = 1 + \Delta h\, z$.

$$\int_0^1 F(\tilde{\sigma}) \left[-2 v_c \tilde{\sigma} + (1-\tilde{\sigma})^2 h \right] dz = 0 \tag{18}$$

where

$$F(\tilde{\sigma}) \equiv \frac{\tilde{\sigma}}{1 - \tilde{\sigma}^2 + 2\tilde{\sigma}^2 \ln \tilde{\sigma}} \tag{19}$$

We can thus solve Eq. (18) for the core velocity in terms of $\tilde{\sigma}$and h only:

$$v_c = \frac{\int_0^1 F(\tilde{\sigma})(1-\tilde{\sigma})^2 h\, dz}{2 \int_0^1 \tilde{\sigma} F(\tilde{\sigma}) dz} \tag{20}$$

Notice that since $0 < \tilde{\sigma} < 1$, $F(\tilde{\sigma})$ is strictly positive and so are both the integrals in Eq. (20). Moreover, by integrating Eq. (17), one finds the pressure difference required to drive the flow:

$$\Delta p = 4 \int_0^1 \frac{v_c + h(1 - \tilde{\sigma} + \tilde{\sigma} \ln \tilde{\sigma})}{h^2 (1 - \tilde{\sigma}^2 + 2\tilde{\sigma}^2 \ln \tilde{\sigma})} dz \tag{21}$$

Therefore, for given volumetric flow-rate, Q, and radius function, $h = h(z)$, one can solve the algebraic/integral Eq. (15) along with Eq. (20) for the radius, $\tilde{\sigma} = \tilde{\sigma}(z)$, and the velocity, v_c, of the unyielded core. Then, Eq. (21) can be used to evaluate the pressure drop, Δp, and the pressure distribution along the pipe by integrating Eq. (17). Finally, the velocity components can be evaluated by means of Eqs. (5) and (8), fully completing the solution of the zero-order problem. Note that a full Newton scheme is utilized to solve Eq. (15) numerically and all integrals are calculated using composite Simpson's rule.

2.1. Approximate solution

Although the zero-order problem has actually been reduced to the algebraic/integral Eq. (15), from the solution of which one can find all the remaining field variables, it is useful to investigate approximate solutions. This can be done as follows. Let the radius of the axisymmetric pipe be of the form

$$h(z) = 1 + \Delta h\, S(z) \tag{22}$$

where $\Delta h \equiv \max_{0 \le z \le 1} h(z) - \min_{0 \le z \le 1} h(z)$ is the amplitude of the wall variation, and $S = S(z)$ is a function which actually describes the deviation from the constant circular cross-section. For small Δh and for fixed Q, we assume a standard power-series expansion of the solution as $X = X_0 + \Delta h X_1 + (\Delta h)^2 X_2 + \ldots$, where $X \in \{v_c,\ \tilde{\sigma},\ p\}$. This expansion is substituted into Eqs. (14)-(16) to obtain a sequence of problems at $O(\Delta h^j)$, $j = 0, 1, 2, \ldots$. The equations are solved analytically up to second order, i.e. up to$O(\Delta h^2)$. The zero-order solution, which corresponds to Poiseuille-flow in a straight pipe, has been reported by Fusi and Farina [12] and Housiadas et al. [7]. This is given concisely in terms of $\tilde{\sigma}_0$:

$$\begin{aligned} Q &= -\frac{1}{3} + \frac{1}{4\tilde{\sigma}_0} + \frac{\tilde{\sigma}_0^3}{12}, \\ v_{c,0} &= -1 + \frac{1}{2\tilde{\sigma}_0} + \frac{\tilde{\sigma}_0}{2}, \\ p_0(z) &= \frac{2(1-z)}{\tilde{\sigma}_0} \end{aligned} \tag{23}$$

From the last expression in Eq. (23), the resulting pressure drop can be found as $\Delta p_0 = 2/\tilde{\sigma}_0$. Since $0 < \tilde{\sigma}_0 < 1$ it is obvious that $\Delta p_0 > 2$. Note that $\tilde{\sigma}_0$ is determined by solving the first expression in Eq. (23), which is a polynomial equation of degree 4. For $Q > 0$, it has one real admissible solution such that $0 < \tilde{\sigma}_0 < 1$. Notice also that the zero-order solution becomes singular as $\tilde{\sigma}_0 \to 0^+$, i.e. when the yield surface approaches the axis of symmetry of the pipe. In this case, all quantities given in Eq. (23) go to infinity, a result which of course is non-physical.

The first-order solution is:

$$v_{c,1} = -\frac{\left(1 - \tilde{\sigma}_0\right)^2 \left(1 + \tilde{\sigma}_0\right)}{\tilde{\sigma}_0 \left(1 + \tilde{\sigma}_0^2\right)} \int_0^1 S(y) dy \tag{24}$$

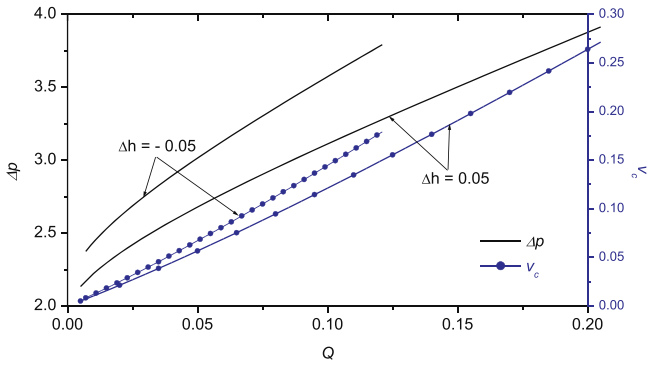

(a)

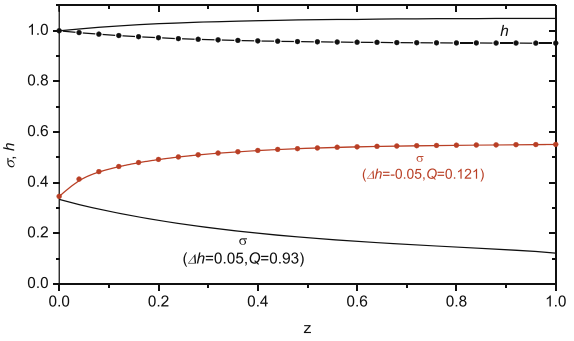

(b)

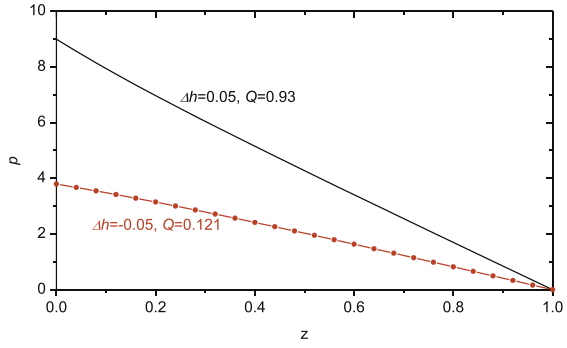

(c)

Fig. 3. Results for exponentially converging/diverging pipes with $\Delta h = \pm 0.05$: (a) Δp(continuous lines) and v_c (lines with dots) vs Q; (b) Yield surfaces for $Q = 0.121(\Delta h = -0.05)$ and $Q = 0.93(\Delta h = 0.05)$; (c) Pressure distributions for $Q = 0.121(\Delta h = -0.05)$ and $Q = 0.93(\Delta h = 0.05)$. The tube radius is given by $h = 1 + \Delta h(1 - e^{-4z})$.

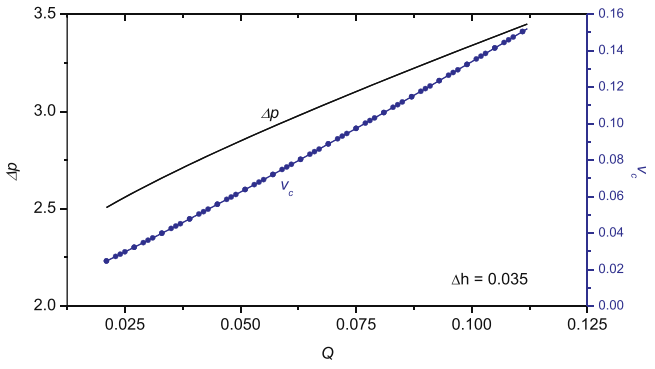

(a)

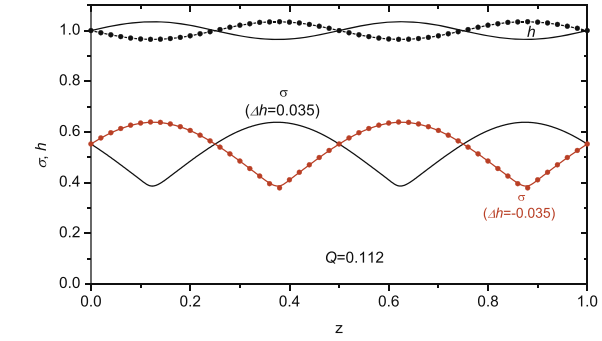

(b)

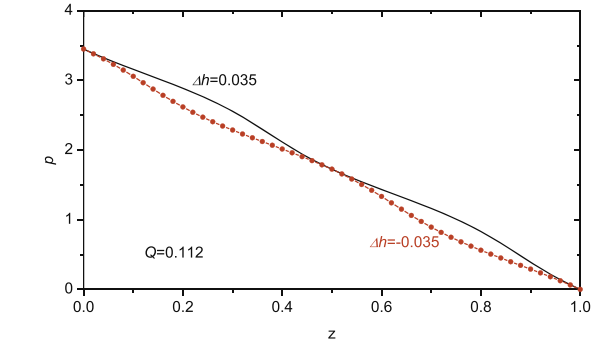

(c)

Fig. 4. Results for wavy pipes with $\Delta h = \pm 0.035$: (a) Δp(continuous line) and v_c (line with dots) vs Q (the results are independent of the sign of Δh); (b) Yield surfaces for $Q = 0.112$; (c) Pressure distributions for $Q = 0.112$. The tube radius is given by $h = 1 + \Delta h \sin(4\pi z)$.

$$\tilde{\sigma}_1(z) = -\frac{\left(1-\tilde{\sigma}_0\right)^3\left(1+\tilde{\sigma}_0\right)^2}{\tilde{\sigma}_0\left(1+\tilde{\sigma}_0^2\right)\left[1-\tilde{\sigma}_0^2+\left(1+\tilde{\sigma}_0^2\right)\ln\tilde{\sigma}_0\right]}\int_0^1 S(y)dy + \frac{\left(1-\tilde{\sigma}_0\right)\left\{\left(1-\tilde{\sigma}_0^2\right)\left(1+\tilde{\sigma}_0+\tilde{\sigma}_0^2\right)+\tilde{\sigma}_0^2\left[\left(3+\tilde{\sigma}_0\left(2+\tilde{\sigma}_0\right)\right)\ln\tilde{\sigma}_0\right]\right\}}{\tilde{\sigma}_0\left(1+\tilde{\sigma}_0\right)\left[1-\tilde{\sigma}_0^2+\left(1+\tilde{\sigma}_0^2\right)\ln\tilde{\sigma}_0\right]}S(z) \tag{25}$$

$$p_1(z) = -\frac{4}{\tilde{\sigma}_0\left[1-\tilde{\sigma}_0^2+\left(1+\tilde{\sigma}_0^2\right)\ln\tilde{\sigma}_0\right]}\left\{\frac{\left(1-\tilde{\sigma}_0^2\right)\left(1-\tilde{\sigma}_0\right)(1-z)}{1+\tilde{\sigma}_0^2}\int_0^1 S(y)dy + \frac{1-\tilde{\sigma}_0^2+2\ln\tilde{\sigma}_0}{1+\tilde{\sigma}_0}\int_z^1 S(y)dy\right\} \tag{26}$$

where the condition $p_1(1) = 0$ has been implemented. By evaluating Eq. (26) at $z = 0$, we find the $O(\Delta h)$ correction to the pressure drop:

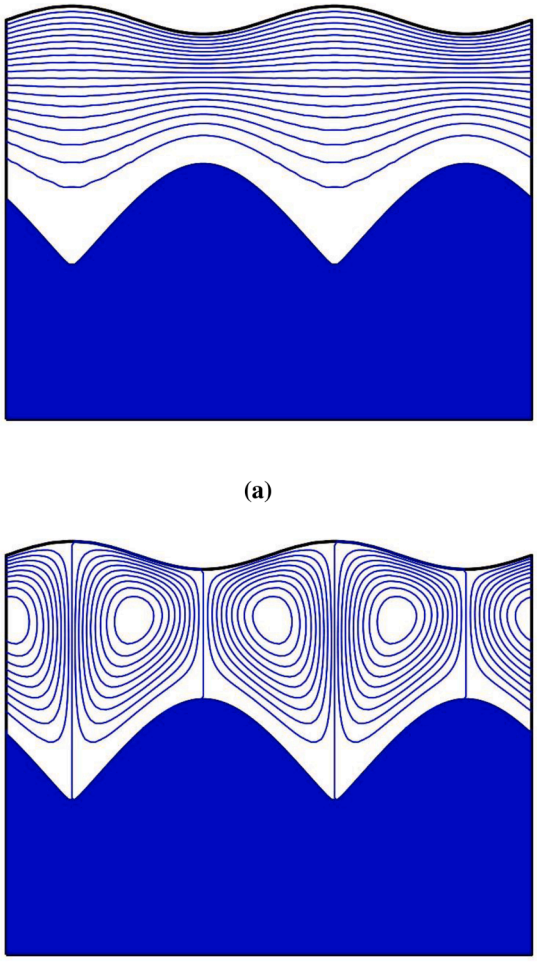

(a)

(b)

Fig. 5. Velocity contours for the undulating tube with $\Delta h = 0.035$ and $Q = 0.112$: (a) v_z (19 uniformly-distributed contour values); (b) v_r (19 uniformly-distributed contour values). The shaded area is the unyielded region. The tube radius is given by $h = 1 + \Delta h \sin(4\pi z)$.

$$\Delta p_1 = -\frac{8}{\tilde{\sigma}_0\left(1+\tilde{\sigma}_0^2\right)\left(1+\tilde{\sigma}_0\right)}\int_0^1 S(y)dy \tag{27}$$

The $O(\Delta h^2)$ solution is too long to be given here.

Eqs. (24)-(27) reveal some interesting features of the solution. For instance, the first correcting term for the yield surface is linear with respect to the shape of wall (not with respect to the axial coordinate). Also, the first-order pressure consists of two parts; the first is linear with respect to the axial coordinate, while the second part depends on the integral of the shape of the wall, S. Also, it is seen that the first-order terms for both the core velocity and the pressure drop depend on the integral $\int_0^1 S(y)dy$. Consequently, a periodic wall-shape can induce only higher-order corrections since $v_{c,\,1}$ and Δp_1 can be zero. Finally, it is worth mentioning that in addition to the singularity observed for the leading order term, a logarithmic singularity is exhibited by $\tilde{\sigma}_1$ as $\tilde{\sigma}_0 \to 0^+$. As discussed in the next Section, this singularity also affects p_1.

3. Results and discussion

First, we point out that for a straight circular pipe, i.e. for $h = 1$, our numerical algorithm produces the correct solution, given by Eq. (23), for

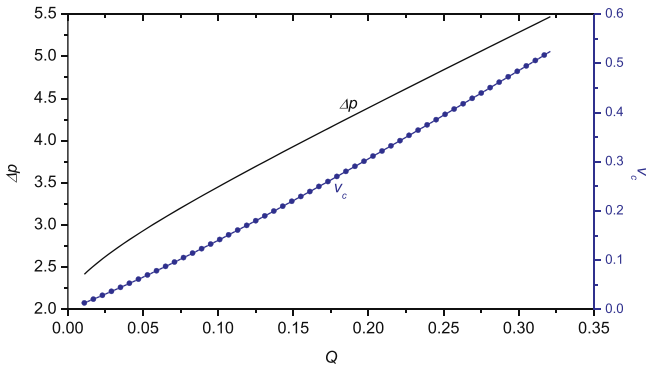

(a)

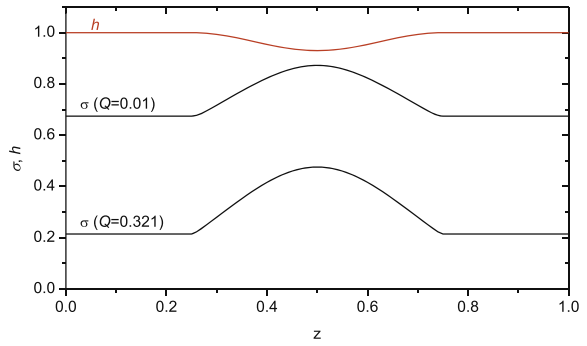

(b)

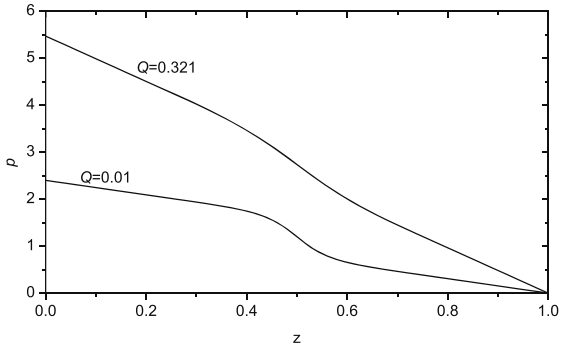

(c)

Fig. 6. Results for a stenosed tube with $\Delta h = 0.035$ and $L_e = 1/4$: (a) Δp (continuous line) and v_c (line with dots) vs Q; (b) Yield surfaces for $Q = 0.01$ and 0.321; (c) Pressure distributions for $Q = 0.01$ and 0.321. The tube radius is given by Eq. (28).

all the variables of interest, and even when the minimum number of points are used (three points). In cases, however, for which $h \neq 1$, and for all the wall shapes that we studied, a convergent solution of Eq. (15) was possible only for small values of Δh. For this reason, we developed a variety of numerical methods to solve Eq. (15), such as a finite difference method, a pseudospectral method, and a finite element method. None of these algorithms was adequate to overcome the convergence problems and thus only small deviations from the constant circular pipe could be studied. In fact, the solution of Eq. (15) is lost at a critical volumetric flow rate, as discussed below. Beyond this critical value the problem is

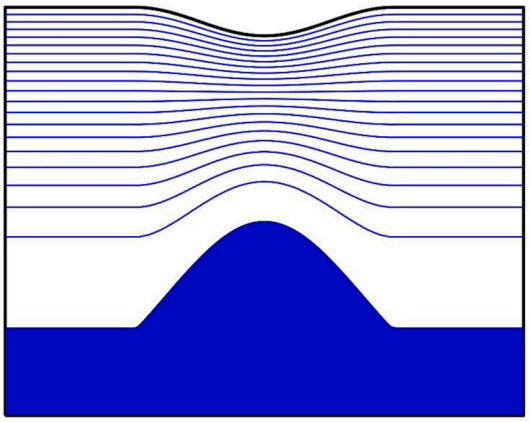

(a)

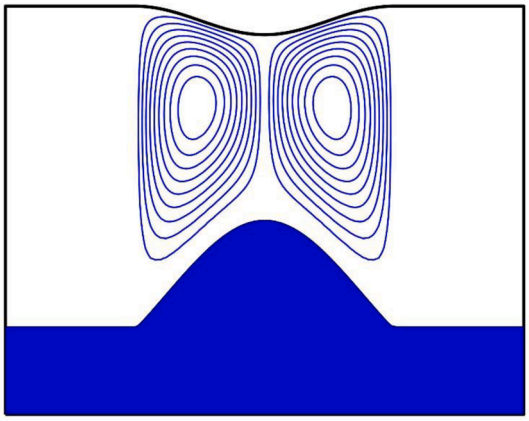

(b)

Fig. 7. Velocity contours for a pipe with a stenosis with $\Delta h = 0.035$ and $Q = 0.321$: (a) v_z (19 uniformly-distributed contour values); (b) v_r (9 positive and 9 negative uniformly-distributed contour values). The shaded area is the unyielded region. The tube radius is given by Eq. (28).

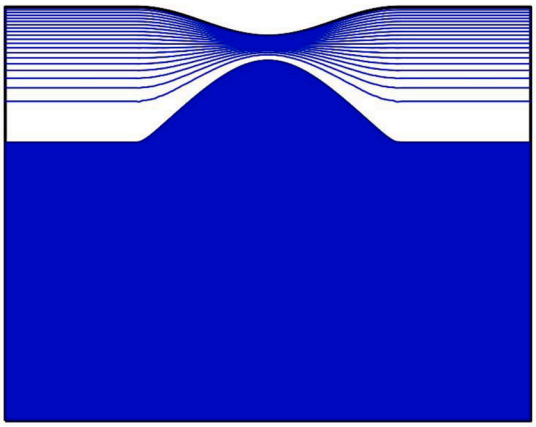

(a)

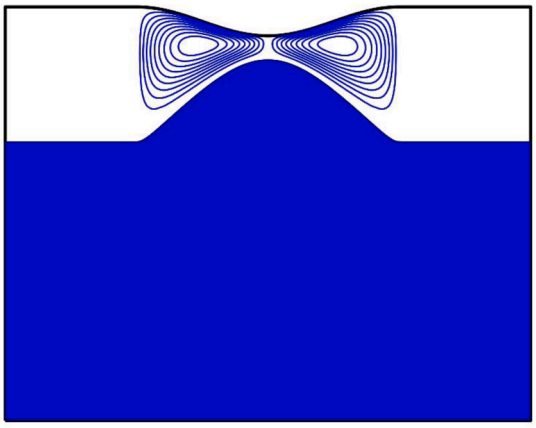

(b)

Fig. 8. Velocity contours for a pipe with a stenosis with $\Delta h = 0.035$ and $Q = 0.01$: (a) v_z (19 uniformly-distributed contour values); (b) v_r (9 positive and 9 negative uniformly-distributed contour values). The shaded area is the unyielded region. The tube radius is given by Eq. (28).

quite stiff in the sense that convergence is achieved only if very small increments of the volumetric flow rate are used. This is of course a limitation of the model (i.e. the zero-order lubrication approximation equations) in cylindrical coordinates.

We consider the flow in linearly diverging and converging tubes, i.e. tubes whose radius is of the form $h = 1 + \Delta h\, z$ (in this case, $S(z) = z$). Fig. 2 shows results obtained with $\Delta h = \pm 0.07$, i.e. for a diverging and a converging pipe. In Fig. 2a, the pressure difference, Δp, and the unyielded core velocity, v_c, are plotted versus the volumetric flow rate, Q. As mentioned in Section I, the method is applicable between the resulting critical values of Δp corresponding to flow-cessation ($\Delta p = 2$) and to plug break-up. We were able to produce convergent numerical results for conditions close to flow-cessation, but not close to plug break-up. Indeed, the solution of Eq. (15) is lost as the volumetric flow rate increases up to a critical point. For instance, the largest values of Q for which a solution was found were 0.182 and 0.111 for the converging and diverging pipes, respectively. The yield surfaces and the pressure distributions for these cases are shown in Fig. 2b and 2c, respectively. It can be observed that in the expanding tube the unyielded core is contracting and vice versa (Fig. 2b). This result, which is dictated by the continuity of mass, is not achieved at zero order with other lubrication methods, which thus exhibit the lubrication approximation paradox. In the expanding tube, the yield surface moves towards the axis of symmetry as Q is increased and eventually the unyielded core breaks at the exit plane. If Q is reduced instead, then the unyielded core moves towards and eventually touches the wall at the inlet, in which case the flow ceases due to the no-slip boundary condition. It should also be pointed out that while the variation of the wall is linear the variation of the yield surface is not and this is a striking difference from the results obtained for the planar channel [6] for which $\sigma = -h(z) + C$ where C is a constant. Last, the results show that as the yield surface moves closer to the axis of symmetry, its gradient becomes steeper at the exit (entrance) of the diverging (converging) pipe and eventually the solution of Eq. (15) is lost.

Other shapes of the wall of the pipe have also been studied. Figs. 3 and 4 show results obtained for tubes with exponentially varying radii following $h = 1 + \Delta h\,(1 - e^{-4z})$ with $\Delta h = \pm 0.05$ and for undulating tubes with radii given by $h = 1 + \Delta h \sin(4\pi z)$ with $\Delta h = \pm 0.035$, respectively. Note that due to the periodicity of the undulating tube, the sign of Δh does not affect the pressure difference,Δp, and the core velocity, v_c (Fig. 4a). The yield surfaces also follow a periodic pattern in phase with the radius function. However, the amplitude of the yield surface variation is greatly intensified as the axis of symmetry is approached and spikes are developed at the points where the yield surface attains minimum values. At the latter points, the derivative of σ eventually becomes discontinuous and the solution of the equation is

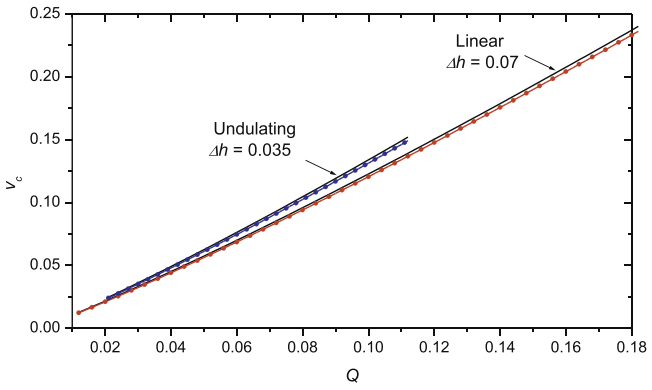

(a)

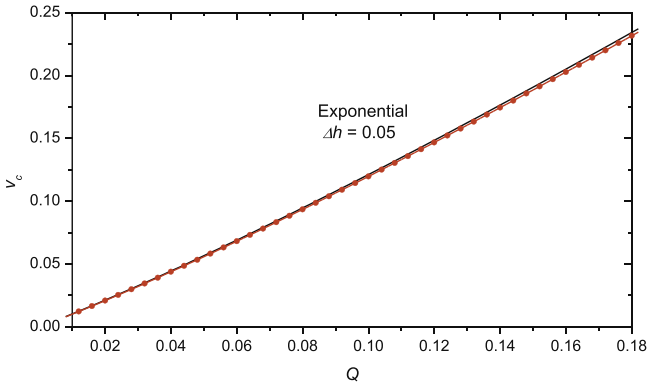

(b)

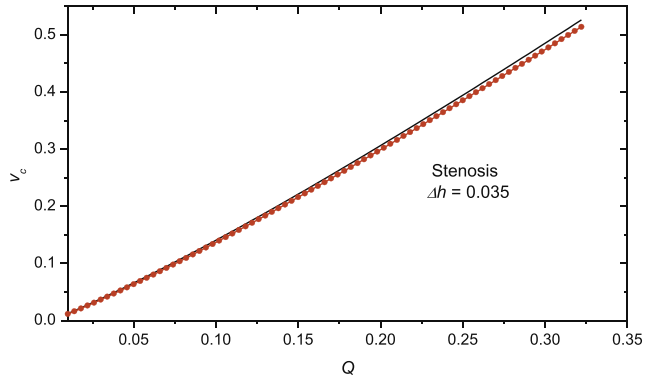

(c)

Fig. 9. Comparison of numerical (solid lines) and approximate (dotted lines) core velocities: (a) Linearly expanding ($\Delta h = 0.07$) and undulating ($\Delta h = 0.035$) tubes; (b) exponentially expanding tube ($\Delta h = 0.05$); (c) stenosed tube with $\Delta h = 0.035$ and $L_e = 1/4$.

lost. The appearance of sharp corners in the unyielded regions in viscoplastic flows is the rule rather than the exception; see for example the patterns in Refs. [18,19] for various flows. In their numerical study of non-Darcy effects in fracture flows of Bingham plastics, Roustaei et al. [20] presented results in wavy channels with broken plugs. However, it can be deduced from their computed examples that if the pressure drop

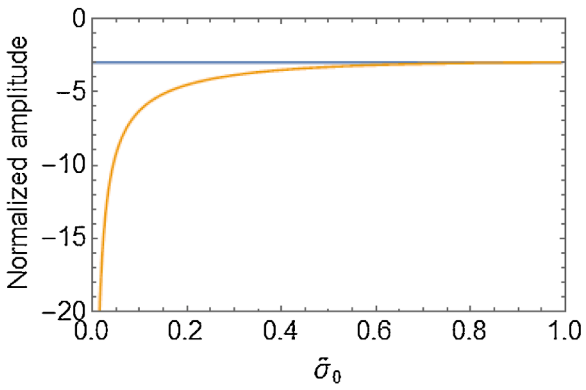

Fig. 10. The normalized amplitude of the variation of the yield surface, i.e. the coefficient of $S(z)$ in Eq. (25). The limit of this coefficient as $\tilde{\sigma}_0 \equiv \sigma_0/h$ tends to unity is -3 (horizontal line).

is reduced the plugs would eventually meet forming sharp corners similar to those predicted by the present lubrication solution. Regarding the pressure distribution, this is almost linear in the exponential case (Fig. 3c), especially at low volumetric flow rates, while in the case of undulating tubes a 'wavy' variation is observed (Fig. 4c). The velocity contours for the case of an undulating tube with $\Delta h = 0.035$ are given in Fig. 5.

We have also considered the flow in a tube with stenosis, which is of interest in hemodynamics. We used the geometry employed by Dimakopoulos et al. [15]. The radius of the stenosed tube is also of the form of Eq. (22):

$$S(z) = \begin{cases} 0, & 0 \le z \le L_e \\ -1 + \cos\left(2\pi \dfrac{z - L_e}{1 - 2L_e}\right), & L_e < z \le 1 - L_e \\ 0, & 1 - L_e < z \le 1 \end{cases} \tag{28}$$

where L_e is a parameter which can vary between 0 and ½ and S is an even function. In Fig. 6, we show the results for $\Delta h = 0.035$ and $L_e = 1/4$. The resulting pressure difference and the core velocity are plotted versus the imposed volumetric flow rate in Fig. 6a, while the yield radius and pressure distributions are shown in Fig. 6b and 6c, respectively. Figs. 7 and 8 show the velocity contours obtained with $Q = 0.321$ and 0.01, respectively. We observe again that the variation of the radius of the unyielded core is enhanced as the volumetric flow rate is increased.

We have also compared the numerical solution with the approximate solution derived in the previous section. In Fig. 9, we plot v_c versus the imposed Q for a linearly diverging pipe with Δh=0.07, an exponentially diverging pipe with Δh=0.05, an undulating pipe with Δh=0.035, and a pipe with stenosis with Δh=0.035. The numerical results are shown with solid lines, while the corresponding perturbation solution $v_c \approx v_{c,0} + \Delta h\, v_{c,1}$ with dotted lines. It is seen that the agreement is very good, for the whole range at which a numerical solution of Eq. (15) can be found. The same holds for the remaining variables (pressure difference, shape of the yield surface, and pressure distribution). Therefore, the expressions given by Eqs. (23)-(27) can safely be used as an approximate solution of Eqs. (13)-(15). Note that the improvement in accuracy when the 2nd-order correction term, $O(\Delta h^2)$, is accounted for is rather marginal.

Due to the very good agreement between the approximate and numerical results, we exploited further the analytical solution in order to investigate the amplification of the variation of the yield surface as the latter approaches the axis of symmetry. Indeed, the normalized amplitude variation (with Δh) is simply given by the coefficient of $S = S(z)$ in Eq. (25). First we note that the limit of this coefficient as $\tilde{\sigma}_0$ goes to one ($\tilde{\sigma}_0 \to 1^-$) is minus three, while as $\tilde{\sigma}_0$ goes to zero ($\tilde{\sigma}_0 \to 0^+$) the limit is

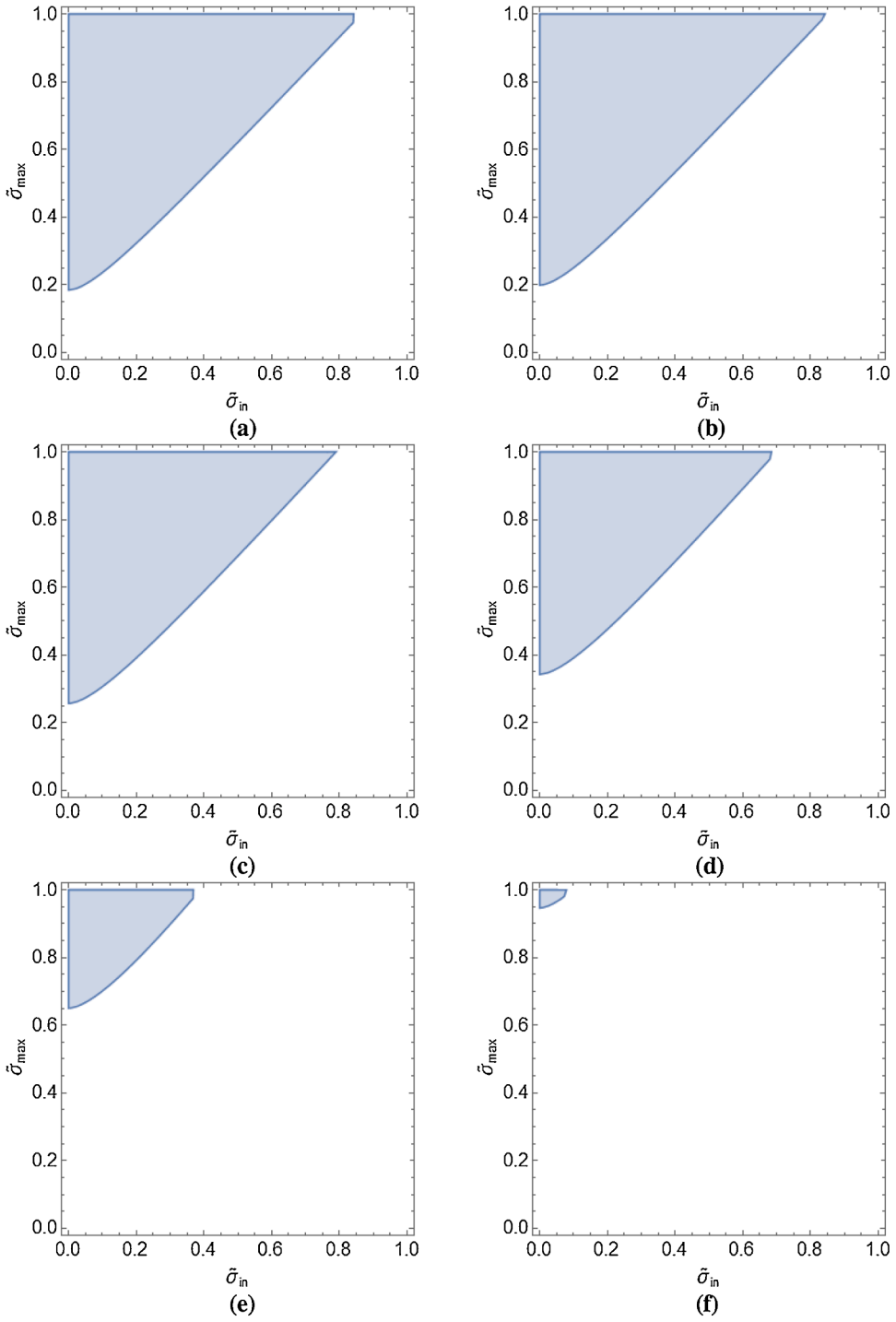

Fig. 11. Regions (shaded) of existence of solutions for Eq. (15) on the $\tilde{\sigma}_{in} - \tilde{\sigma}_{max}$ plane, where $\tilde{\sigma}_{in} = \tilde{\sigma}(0)$ and $\tilde{\sigma}_{max}$ is the maximum radius of the unyielded core (which corresponds to the minimum of the tube radius). The solution is lost at $\Delta h \sim 0.29$: (a) $\Delta h = 0.035$; (b) $\Delta h = 0.05$; (c) $\Delta h = 0.07$; (d) $\Delta h = 0.1$; (e) $\Delta h = 0.2$; (f) $\Delta h \sim 0.28$.

minus infinity. Thus, the approximate solution will inevitably fail under flow conditions where the yield surface approaches the axis of symmetry, since in this case the first-correction term $\tilde{\sigma}_1$ dominates on the leading-order term (i.e., on $\tilde{\sigma}_0$). Indeed, this can be seen in Fig. 10, where the normalized amplitude of the yield surface variation is plotted versus $\tilde{\sigma}_0 \equiv 2/\Delta p_0$. It is quite interesting that in the region $0.4 < \tilde{\sigma}_0 < 1$ the amplitude decreases smoothly and very little from its asymptotic value -3, while a fast decrease is observed for $\tilde{\sigma}_0 < 0.4$; note that at the value 0.4 the numerical code also fails to converge. Therefore, it can be deduced that the logarithmic singularity predicted by the approximate solution (see Eqs. (25) and (26)) is not due to the method of solution but an actual feature of the mathematical model used here, i.e. of the lubrication approximation for a very long pipe with variable radius.

Finally, we investigate the existence of solutions of Eq. (15) for converging tubes, graphically, as follows. First, we denote the reduced radii of the unyielded core at the entrance of the tube (where $h = 1$) by $\tilde{\sigma}_{in} \equiv \sigma/h|_{h=1}$. Then, Eq. (15) gives:

$$Q = \frac{\left(1-\tilde{\sigma}_{in}\right)^2\left[\left(1+\tilde{\sigma}_{in}\right)^2 v_c + \frac{1}{3}\left(1+2\tilde{\sigma}_{in}\right)\left(1-\tilde{\sigma}_{in}^2\right) + \frac{\tilde{\sigma}_{in}}{3}\left(3+2\tilde{\sigma}_{in}+\tilde{\sigma}_{in}^2\right)\ln\tilde{\sigma}_{in}\right]}{2\left(1-\tilde{\sigma}_{in}^2+2\tilde{\sigma}_{in}^2\ln\tilde{\sigma}_{in}\right)} \tag{29}$$

Recalling that the maximum value of the yield surface is achieved when the radius of the tube is at minimum, i.e. $h = 1 - \Delta h$, and denoting the corresponding reduced radii of the unyielded core as $\tilde{\sigma}_{\max} \equiv \sigma/h|_{h=1-\Delta h}$, Eq. (15) yields:

$$Q = \frac{\left(1-\tilde{\sigma}_{\max}\right)^2(1-\Delta h)^3\left[\left(1+\tilde{\sigma}_{\max}\right)^2 \frac{v_c}{1-\Delta h} + \frac{1}{3}\left(1+2\tilde{\sigma}_{\max}\right)\left(1-\tilde{\sigma}_{\max}^2\right) + \frac{\tilde{\sigma}_{\max}}{3}\left(3+2\tilde{\sigma}_{\max}+\tilde{\sigma}_{\max}^2\right)\ln\tilde{\sigma}_{\max}^2\right]}{2\left(1-\tilde{\sigma}_{\max}^2+2\tilde{\sigma}_{\max}^2\ln\tilde{\sigma}_{\max}\right)} \tag{30}$$

Since Q is constant, Eqs. (29) and (30) can be used to find the constant core velocity v_c in terms of $\tilde{\sigma}_{in}$,$\tilde{\sigma}_{\max}$ and Δh, i.e. $v_c = v_c(\tilde{\sigma}_{in},\tilde{\sigma}_{\max},\Delta h)$. Obviously, a solution of Eq. (15) exists as long as $\tilde{\sigma}_{\max} > \tilde{\sigma}_{in}$ and $v_c > 0$. In Fig. 11, the shaded areas represent the regions where both conditions are met on the $\tilde{\sigma}_{in} - \tilde{\sigma}_{\max}$ plane ($0 \le \tilde{\sigma}_{\max}, \tilde{\sigma}_{in} \le 1$) for $\Delta h = 0.035, 0.05, 0.07, 0.1, 0.2$ and 0.28. One can observe that as Δh increases this region shrinks and eventually, at $\Delta h \approx 0.29$, disappears, which mean that the solution of Eq. (15) is lost. Therefore, we conclude that a solution of Eq. (15) exists only up to a certain value of Δh. The same analysis can be performed also for diverging pipes too and leads to similar results.

4. Conclusions

A lubrication solution for the flow of a Bingham fluid in a tube of variable radius has been obtained under the assumption that the unyielded core extends continuously from the inlet to the outlet of the tube. The problem is reduced to solving a stiff algebraic/integral equation for the radius of the unyielded core. The pressure distribution and the velocity components are then calculated using explicit analytical expressions. With the proposed method, the lubrication approximation paradox is avoided at the leading order of approximation, i.e. the predicted radius of the unyielded core diverges in a converging channel and vice versa. Results have been obtained for different geometries, i.e. for linearly or exponentially diverging or converging tubes and for undulating and stenosed tubes. In contrast to the planar geometry, where the shape of the unyielded core depends solely on the width of the channel, in the axisymmetric flow the shape of the unyielded core also depends on the imposed pressure difference. The higher the pressure difference the more pronounced the effect of the tube radius on the unyielded core, which explains the stiffness of the problem as the yield surface approaches the symmetry axis. Our calculations showed that the pressure difference for the converging pipe is always larger that for the diverging pipe.

An approximate analytical solution has also been derived as a check to the lubrication solution. Both solutions reveal that the effect of the amplitude of the wall variation is greatly amplified as the volumetric flow-rate increases, i.e. as the yield surface moves closer to the symmetry axis. A logarithmic singularity of the solution is also revealed analytically. The latter causes the loss of uniform convergence of the perturbation solution as well as to the divergence of the numerical code as the yield surface approaches the symmetry axis of the pipe.

Declaration of Competing Interest

The Authors declare that there is no conflict of interest.

References

[1] P. Coussot, Slow flows of yield stress fluids: yielding liquids or flowing solids, Rheol. Acta 57 (2018) 1–14.
[2] I. Frigaard, Simple yield-stress fluids, Curr. Opinion Coll. Inter. Sci. 43 (2019) 80–93.
[3] D. Bonn, J. Paredes, M.M. Denn, L. Berthier, T. Divoux, S. Manneville, Yield stress materials in soft condensed matter, Rev. Mod. Phys. 89 (2017), 035005.
[4] N.J. Balmforth, I.A. Frigaard, G. Ovarlez, Yielding to stress: recent developments in viscoplastic fluid mechanics, Annu. Rev. Fluid Mech. 46 (2014) 121–146.
[5] E.C. Bingham, Fluidity and Plasticity, McGraw Hill, New-York, 1922.
[6] P. Panaseti, Y. Damianou, G.C. Georgiou, K.D. Housiadas, Pressure-driven flow of a Herschel-Bulkley fluid with pressure-dependent rheological parameters, Physics of Fluids 30 (2018), 030701.
[7] K.D. Housiadas, I. Ioannou, G.C. Georgiou, Lubrication solution of the axisymmetric Poiseuille flow of a Bingham fluid with pressure-dependent rheological parameters, J. Non-Newtonian Fluid Mech 260 (2018) 76–86.
[8] L. Fusi, A. Farina, F. Rosso, S. Roscani, Pressure-driven lubrication flow of a Bingham fluid in a channel: a novel approach, J. Non-Newtonian Fluid Mech 221 (2015) 66–75.
[9] A. Putz, I.A. Frigaard, D.M. Martinez, On the lubrication paradox and the use of regularization methods for lubrication flows, J. Non-Newtonian Fluid Mech 163 (2009) 62–77.
[10] I.A. Frigaard, D.P. Ryan, Flow of a visco-plastic fluid in a channel of slowly varying width, J. Non-Newtonian Fluid Mech 123 (2004) 67–83.
[11] P. Panaseti, G.C. Georgiou, I. Ioannou, Lubrication solution of the flow of a Herschel-Bulkley fluid with pressure-dependent rheological parameters in an asymmetric channel, Physics of Fluids 31 (2) (2019), 023106.

[12] L. Fusi, A. Farina, Peristaltic axisymmetric flow of a Bingham plastic, Appl. Math. Comp 320 (2018) 1–15.
[13] P. de Souza Mendes, M. Naccache, P. Varges, F. Marchesini, Flow of viscoplastic liquids through axisymmetric expansions-contractions, J. Non-Newtonian Fluid Mech 142 (2007) 207–217.
[14] L. Hermany, D. Dall'Onder dos Santos, S. Frey, M. Naccache, P. de Souza Mendes, Flow of yield-stress fluids through an axisymmetric abrupt expansion-contraction, J. Non-Newtonian Fluid Mech 201 (2013) 35–52.
[15] Y. Dimakopoulos, G. Kelesidis, S. Tsouka, G.C. Georgiou, J. Tsamopoulos, Hemodynamics in stenotic microvessels under steady state conditions. Part I: the non-homogeneous model, J. Biorheology 52 (3) (2015) 183–210.
[16] M.P. Dalwadi MP, I.M. Griffiths, M. Bruna, Understanding how porosity gradients can make a better filter using homogenization theory, Proc. R. Soc. A 471 (2015), 20150464. https://doi.org/10.1098/rspa.2015.0464.
[17] M. Veyskarami, A.H. Hassani, M.H. Ghazanfari, Modeling of non-Darcy flow through anisotropic porous media: role of pore space profiles, Chem. Eng. Sci. 151 (2016) 93–104.
[18] A. Syrakos, G.C. Georgiou, A.N. Alexandrou, Performance of the finite volume method in solving regularised Bingham flows: inertia effects in the lid-driven cavity flow, J. non-Newtonian Fluid Mech 208-209 (2014) 88–107.
[19] Y. Dimakopoulos, G. Makrigiorgos, G.C. Georgiou, J. Tsamopoulos, The PAL (Penalized Augmented Lagrangian) Method for Computing Viscoplastic Flows: a New Fast Converging Scheme, J. Non-Newtonian Fluid Mech. 236 (2018) 23–51.
[20] A. Roustaei, T. Chevalier, L. Talon, I.A. Frigaard, Non-Darcy effects in fracture flows of a yield stress fluid, J. Fluid Mech 805 (2016) 222–261.